Pro-1 of Macrophage Migration Inhibitory Factor Functions as a Catalytic Base in the Phenylpyruvate Tautomerase Activity[†,‡]

Jodi B. Lubetsky,[§,⊥] Melissa Swope,[§] Chris Dealwis,[§] Paul Blake,[∥] and Elias Lolis*[,§]

Departments of Pharmacology and Molecular Biophysics and Biochemistry, Yale University School of Medicine, New Haven, Connecticut 06510, and Department of Chemistry, Pharmaceutical Division, Bayer Corporation, West Haven, Connecticut 06516

Received February 9, 1999; Revised Manuscript Received April 6, 1999

ABSTRACT: Macrophage migration inhibitory factor (MIF) is an important immunoregulatory molecule with a unique ability to suppress the anti-inflammatory effects of glucocorticoids. Although considered a cytokine, MIF possesses a three-dimensional structure and active site similar to those of 4-oxalocrotonate tautomerase and 5-carboxymethyl-2-hydroxymuconate isomerase. Moreover, a number of catalytic activities have been defined for MIF. To gain insight into the role of catalysis in the biological function of MIF, we have begun to characterize the catalytic activities in more detail. Here we report the crystal structure of MIF complexed with *p*-hydroxyphenylpyruvate, a substrate for the phenylpyruvate tautomerase activity of MIF. The three binding sites for *p*-hydroxyphenylpyruvate in the MIF trimer lie at the interface between two subunits. The substrate interacts with Pro-1, Lys-32, and Ile-64 from one subunit and Tyr-95 and Asn-97 from an adjacent subunit. Pro-1 is positioned to function as a catalytic base. There is no functional group that polarizes the α-carbonyl of the substrate to weaken the adjacent C−H bond. Mutation of Pro-1 to glycine substantially reduces the catalytic activity. The insertion of an alanine between Pro-1 and Met-2 essentially abolishes activity. Structural studies of these mutants define a source of the reduced activity and provide insight into the mechanism of the catalytic reaction.

Macrophage migration inhibitory factor (MIF)[1] is an immunoregulatory protein that has been associated with a range of biological activities both within and outside the immune system (*1*−*4*). Although neither a receptor nor a high-affinity binding site has been identified for MIF, the protein has been classified as a cytokine. Some of its biological activities include inhibition of macrophage migration, an activity associated with general macrophage activation and delayed-type hypersensitivity reactions (*5*−*7*), and suppression of glucocorticoid-induced inhibition of cytokine production from macrophages (*8*). Neutralization of MIF by anti-MIF antibodies was shown to be therapeutically beneficial in a variety of animal models of proinflammatory diseases, including sepsis (*9*, *10*), adult respiratory distress syndrome (*11*), rheumatoid arthritis (*12*), and glomerulonephritis (*13*). Gene deletion studies with mice confirm an important role for MIF in sepsis and lung inflammatory disease (*14*).

Recently, several studies have reported a variety of catalytic activities for MIF including D-dopachrome tautomerase (*15*), phenylpyruvate tautomerase (*16*), and protein-thiol oxidoreductase (*17*). The significance of these catalytic activities to the physiological function of MIF is unknown. It is important to note that D-dopachrome is not a physiological molecule (*15*). Values for the Michaelis constant (K_m) of phenylpyruvate or hydroxyphenylpyruvate have been reported to be too high for these molecules to serve as physiological substrates (*16*). However, K_m values are not good indicators of the physiological significance of enzyme−substrate pairs, and further studies are required to address this issue.

The three-dimensional structure of MIF has been determined to high resolution (*18*, *19*). MIF crystallizes as a trimer of three identical subunits. The structure of MIF supports a catalytic function for this protein. The structure of MIF is similar to those of two bacterial enzymes [5-carboxymethyl-2-hydroxymuconate isomerase (CHMI) and 4-oxalocrotonate tautomerase (4-OT)] and shares an N-terminal proline that CHMI and 4-OT utilize as a catalytic base (*18*−*22*). The N-terminal proline (Pro-1) of MIF is required for the D-dopachrome tautomerase and phenylpyruvate tautomerase activities (*23*) and is modified by an active site-directed irreversible inhibitor (*24*). The protein-thiol oxidoreductase activity is mediated by cysteines located elsewhere on the structure (*25*). Pro-1 is also required for at least one of the cytokine activities of MIF, suggesting that an active site-directed inhibitor may mimic the therapeutic effects of anti-MIF antibodies (*23*).

[†] This research was partly supported by a grant from Connecticut Innovations, Inc.

[‡] The coordinates have been deposited with Brookhaven Protein Data Bank (PDB codes 1CA7, 1P1G, and 1CGQ).

* To whom correspondence should be addressed. Telephone: (203) 785-6233. Fax: (203) 785-7670. E-mail: elias.lolis@yale.edu.

[§] Department of Pharmacology, Yale University School of Medicine.

[⊥] Department of Molecular Biophysics and Biochemistry, Yale University School of Medicine.

[∥] Bayer Corporation.

[1] Abbreviations: MIF, macrophage migration inhibitory factor; 4-OT, 4-oxalocrotonate tautomerase; CHMI, 5-carboxymethyl-2-hydroxymuconate isomerase; HPP, *p*-hydroxyphenylpyruvate; HSQC, heteronuclear single-quantum coherence.

10.1021/bi990306m CCC: $18.00
Published on Web 05/11/1999

While the importance of Pro-1 in MIF has been demonstrated, its actual role is in question. It has been proposed to serve as a catalytic acid in the D-dopachrome tautomerase activity (*25*) and as a catalytic base in the phenylpyruvate tautomerase activity (*23*, *24*). The environment at the active site reduces the pK_a of the N-terminal proline by almost 4 pH units relative to that of a proline amide (*22*), suggesting that Pro-1 could function as a catalytic base at physiological pH (*23*, *24*). To understand the structural, stereochemical, and mechanistic basis of the phenylpyruvate tautomerase activity, we report the crystal structure of the complex between MIF and the substrate *p*-hydroxyphenylpyruvate (HPP). To further define the role of Pro-1, we have created and characterized two N-terminal mutants. The replacement of proline by glycine (P1G) has been previously reported and shown to link the catalytic active site with the neutrophil-priming activity of MIF (*23*). In the second mutant, an alanine is inserted between Pro-1 and Met-2 (PAM), resulting in the movement of the proline from the catalytic pocket. We report the biochemical and structural properties for each mutant. These results enable us to better understand the mechanism of the isomerization reaction catalyzed by MIF and the role of Pro-1.

EXPERIMENTAL PROCEDURES

Materials and Strains. PCR reagents, restriction enzymes, and T4 DNA ligase were purchased from New England Biolabs (Beverly, MA). Oligonucleotides were synthesized at the Keck Oligonucleotide Synthesis Facility at Yale University. Agarose was obtained from Bio-Rad Laboratories (Hercules, CA). QuicKit for DNA purification of PCR products was obtained from National Scientific Supply Company, Inc. (San Rafael, CA). Plasmid preps were performed using a QIAGEN Midi Kit (Santa Clarita, CA). Tryptone, yeast extract, and Bacto-agar were purchased from Difco (Detroit, MI). Ampicillin and Tris were purchased from American Bioanalytical (Natick, MA). IPTG and Hepes were purchased from Boehringer Mannheim (Indianapolis, IN). Protamine sulfate, biotin, PEG 400, and *p*-hydroxyphenylpyruvic acid were purchased from Sigma (St. Louis, MO). Cellulose acetate filter units were obtained from Corning (Corning, NY). The YM-10 ultrafiltration membranes and Centricon (10 000 MW cutoff) centrifugal microconcentrators were obtained from Amicon (Bedford, MA). [^{15}N]Ammonium sulfate was obtained from Cambridge Isotope Laboratories (Andover, MA), and ^{15}N-labeled Celtone was purchased from Martek (Columbia, MD). Both thiamine hydrochloride and thymidine were purchased from GibcoBRL (Grand Island, NY). Iron(III) chloride hexahydrate was obtained from Aldrich (Milwaukee, WI). All other reagents and buffers were obtained from J. T. Baker (Phillipsburg, NJ).

Competent *Escherichia coli* (strain DH5α) cells were purchased from GibcoBRL (Gaithersburg, MD). *E. coli* strain BL21(DE3) was obtained from Novagen (Madison, WI) and used for the expression of recombinant proteins.

Mutagenesis of MIF and DNA Sequencing. The P1G mutant cDNA was generated by PCR using the primer 5′-GCATATA**CATATG***GGC*ATGTTCATCGTA-3′ that encodes an *Nde*I restriction site (bold) and a codon for glycine (italics) instead of a proline after the initiating methionine. The second primer 5′-TT**GGATCC**TTAGGCGAAGGTGGAGTT-3′ was annealed to the 3′ end of the wild-type cDNA and contained a *Bam*HI restriction site (bold). The PAM mutant cDNA was generated by PCR using the primer 5′-GCATATA**CATATG**CCG*GCG*ATGTTCATCGTA-3′ that encodes an *Nde*I restriction site (bold) and a codon for alanine (italics) between the codons for Pro-1 and Met-2. The second primer is the same as that for the P1G mutant.

PCRs were carried out on a Minicycler (MJ Research, Inc., Watertown, MA). Each 50 μL reaction mixture contained Vent polymerase buffer, dNTPs (1 μL of a 10 mM dNTP mix), Vent DNA polymerase (1 μL of a 2 units/μL solution), primers (1 μL each of 100 μM stocks), and 2−3 ng of template DNA (wild-type MIF in a pET11b vector). Thirty cycles of amplification were carried out, each cycle consisting of denaturation at 94 °C for 1 min, annealing at 55 °C for 1 min, and elongation at 72 °C for 1 min. The PCR products were purified via low-melt agarose gel extraction. Restriction digests were then performed by incubation at 37 °C for 1−2 h with the appropriate enzymes. DNA fragments were again purified, and an overnight ligation with *Nde*I−*Bam*HI-cleaved pET-11b was performed at 16 °C. The ligation mix was transformed into *E. coli* DH5α competent cells and grown on LB-ampicillin plates (100 μg/mL) using standard methods (*26*). Single colonies were used to inoculate LB-ampicillin media, from which plasmid DNA was purified and used for sequencing. DNA sequencing was carried out on an Applied Biosystems 377 DNA sequencer utilizing fluorescently labeled dideoxynucleotides (dRhodamine Terminators) and Taq FS DNA polymerase in a thermal cycling protocol. Plasmids with the correct sequence were transformed into *E. coli* strain BL21(DE3) for protein expression.

Expression and Purification of MIF. Expression and purification of the proteins were performed as previously described (*23*, *27*). Briefly, expression of the wild type and mutant protein involved growing pET11b-MIF-transformed BL21(DE3) cells to an OD_{600} of 0.7−1.0 and inducing with IPTG to a final concentration of 1 mM. After growth for 5 h, the cells were harvested and resuspended in 20 mM Tris and 20 mM NaCl (pH 7.5) at 7−14% of the original volume of growth media. Cells were lysed using a French press. After addition of protamine sulfate to a final concentration of 0.006%, cell debris was removed by centrifugation at 27000*g* for 30 min. The supernatant was filtered using a 0.22 μm cellulose acetate filter and then applied to a Mono S and a Mono Q (Pharmacia, Piscataway, NJ) anion-exchange column. Under the buffer conditions that were used, most contaminating proteins adsorbed to one of the chromatographic media, whereas wild-type and mutant MIF did not. The fractions containing MIF were pooled and concentrated using ultrafiltration and microconcentrators. Protein concentrations were determined by measuring absorbance at 280 nm ($\epsilon = 1.22$ mg^{-1} mL cm^{-1}). The resulting MIF sample was >95% pure and suitable for catalytic characterization, NMR spectroscopy, and X-ray crystallography.

[^{15}N]MIF was prepared in minimal media containing 47.9 mM Na_2HPO_4, 22 mM KH_2PO_4, 8.6 mM NaCl, 7.5 mM $(^{15}NH_4)_2SO_4$, 22.2 mM glucose, 1.99 mM $MgSO_4{\cdot}7H_2O$, 100 μM $CaCl_2{\cdot}2H_2O$, 26 μM $FeCl_3{\cdot}6H_2O$, 60 μM thiamine hydrochloride, 82.5 μM thymidine, 10% ^{15}N-labeled Celtone (1×), 2.5 μM biotin, and 100 μg/mL ampicillin (*23*). An overnight 25 mL culture of the wild type or mutant pET11b MIF in BL21(DE3) cells was added to 250−500 mL of

labeled minimal media in a baffle flask and grown at 37 °C until the culture reached an OD_{600} of 0.7−1.0. IPTG was added to a final concentration of 1 mM, and the cells were induced overnight. For purification, we followed the same method described above.

N-Terminal Sequencing and Mass Spectrometry. Amino terminal sequencing was carried out on an Applied Biosystems sequencer equipped with an on-line HPLC system at the Keck Foundation Biotechnology Resource Laboratory. Five cycles of sequencing were carried out to identify the amino acid sequence. For mass spectrometry, samples were further purified using a Vydec C4 column and eluted with a gradient of 30 to 80% acetonitrile in 0.1% trifluoroacetic acid. Samples were diluted into 2-propanol and water (1:1, v/v) with 0.1% formic acid and analyzed on a VG Quattro (Fisons Instruments) triple-quadropole mass spectrometer equipped with an electrospray ion source.

Hydroxyphenylpyruvate Tautomerase Assays. For phenylpyruvate tautomerase assays, we used *p*-hydroxyphenylpyruvate (HPP) as the substrate. HPP was dissolved in 50 mM ammonium acetate (pH 6.0), allowed to equilibrate at room temperature overnight, and stored at 4 °C. Catalytic activity was initiated at 25 °C by adding HPP to a quartz cuvette containing MIF and 0.435 M boric acid (pH 6.2). Activity was measured by following the increase in absorbance at 330 nm for 5−40 s due to the formation of the borate−enol complex. The concentration of MIF used for the catalytic assay was 10 nM for the wild-type protein, 1.2 μM for P1G, and 15 μM for PAM. All initial rates were corrected for background by performing the assay at each HPP concentration without MIF and subtracting the uncatalyzed rate from the initial rate in the presence of MIF.

NMR Studies. One-dimensional ^{15}N spectra were collected with 2−3 mM samples of wild-type or mutant [^{15}N]MIF in 20 mM phosphate buffer containing 200 mM NaCl. The pH was adjusted to the appropriate value by addition of 0.5−2 μL additions of 0.1−1.0 N NaOH or HCl. All measurements were taken on a Bruker DMX500 using a 5 mm broad-band probe with the following acquisition parameters: spectrometer frequency, 50.648 MHz; spectral width, 11 468 Hz; acquisition time, 714 ms; relaxation delay, 100 ms; 25−90K total transients; and temperature, 295 K. $^{1}H-^{15}N$ HSQC two-dimensional spectra were recorded for 1−2 mM samples in 20 mM phosphate buffer (pH 6.8) using a Bruker 5 mm triple-resonance probe with three-axis gradients. Acquisition parameters were as follows: spectrometer frequency, 600.139 MHz; spectral width, 5388 Hz; acquisition time, 95 ms; recycle delay, 1 s; transients per block, 32; complex blocks, 128; and temperature, 298 K. To facilitate sample locking, 5% D_2O was added to all samples.

Crystallography. Wild-type MIF, P1G, and PAM were concentrated to 10−15 mg/mL before crystallization. Crystals were grown using the hanging drop vapor diffusion method. For crystals of P1G and PAM, equal volumes (1 μL) of protein and reservoir solution [2.0 M ammonium sulfate/2% PEG 400/0.1 M Hepes (pH 7.5)] were mixed and allowed to equilibrate at room temperature. Crystals appeared within a few days. P1G crystals belong to space group $P3_121$ with the following unit cell dimensions: $a = b = 95.81$ Å and $c = 104.16$ Å. PAM crystals belong to space group $P2_12_12_1$ with the following unit cell dimensions: $a = 67.81$ Å, $b = 67.87$ Å, and $c = 88.77$ Å. For the MIF−HPP cocrystals, equal volumes (1 μL) of protein and 100 mM HPP dissolved in reservoir solution [2.0 M ammonium sulfate/4% 2-propanol/0.1 M Tris (pH 8.0)] were mixed. Wild-type MIF−HPP crystals belong to space group $P2_12_12_1$ with the following unit cell dimensions: $a = 68.04$ Å, $b = 67.85$ Å, and $c = 87.93$ Å.

All crystals were equilibrated with cryoprotectant (25% glycerol in mother liquor) for 10−15 min and were frozen rapidly in a stream of N_2 at −140 °C for data collection. Diffraction data were collected on an RAXIS-IIC image plate detector (Rigaku, Tokyo, Japan) with a Rigaku RU200 rotating anode X-ray generator. Data were processed by the DENZO/SCALEPACK package (*28*) and CCP4 (*29*).

The structure of the orthorhombic crystal form of wild-type MIF complexed with *p*-hydroxyphenylpyruvate was determined by molecular replacement with AMORE (*30*) using the monomer structure of uncomplexed MIF (*31*). Refinement was performed with X-PLOR 3.851 (*32*). The R_{free} was implemented in the beginning of refinement and used throughout the refinement process as a guide for model improvement (*33*). The graphics program O (*34*) was used for the display of electron density maps. After rigid body refinement, a series of positional refinement rounds were performed in which strict noncrystallographic symmetry (NCS) constraints were implemented. The enol form of HPP was built into the electron density of a simulated annealing omit map calculated with NCS averaging. [The coordinates, topology, and parameter files for the enol form of *p*-hydroxyphenylpyruvate were constructed with INSIGHTII (Molecular Simulations, Inc., San Diego, CA) and XPLOR2D (*35*).] Grouped *B*-factor refinement, individual *B*-factor refinement, and bulk solvent correction, which enabled the use of lower-resolution data throughout the subsequent rounds of refinement, were implemented. The trimer was generated, and further rounds of NCS-restrained refinement and model building were performed to obtain the final structure.

The structures of P1G and PAM mutants were determined by Fourier differences using phases from uncomplexed MIF (for P1G) and MIF from the MIF−HPP complex (for PAM). In each case, the N-terminal residue was deleted from the phase calculation. Following initial rigid body refinement, a simulated annealing omit map was constructed to help rebuild the N-terminal residue of the structure. Subsequent refinement was performed essentially as described above for the MIF−HPP structure. Data and refinement statistics for all structures are listed in Table 1. Errors for each structure were estimated by the method of Luzzati (*36*).

RESULTS

Protein Expression and Characterization. The cDNA sequences of both the P1G and PAM mutants were constructed by PCR and confirmed by dideoxy sequencing. Both mutants were expressed and purified from *E. coli* BL21-(DE3) cells on the basis of the protocol that was developed for wild-type MIF (*27*). The final yield of the two mutants and wild-type MIF from BL21(DE3) was approximately 40 mg/L. Mass spectrometry was performed on each purified protein product. The molecular masses for the wild type, P1G, and PAM MIF were 12 345, 12 302, and 12 415 Da, respectively (Figure 1). These values are all within 2.5 Da of the predicted molecular mass for each protein, assuming

Table 1: Crystal Parameters and Data and Refinement Statistics[a]

	MIF−HPP	P1G	PAM
crystal parameters			
space group	$P2_12_12_1$	$P3_121$	$P2_12_12_1$
unit cell dimensions (a, b, c) (Å)	68.0, 67.9, 87.9	95.8, 95.8, 104.2	67.8, 67.9, 88.8
data statistics			
resolution (Å)	2.5	2.5	2.0
no. of collected reflections	137711	50378	115296
no. of unique reflections	15313	18195	27733
completeness (total/high) (%)	95.2/73.8	93.7/94.8	98.2/96.8
R_m (total/high) (%)[b]	9.4/33	4.9/10.5	7.8/9.4
$\langle I/\sigma(I)\rangle$ (total/high)	5.3/2.5	6.5/6.4	6.0/6.2
refinement statistics			
resolution range (Å)	20−2.5	20−2.5	20−2
no. of reflections with $F > 2\sigma(F)$	14006	18017	27635
no. of protein atoms	2601	2592	2616
no. of water molecules	18	33	111
no. of other atoms	39	−	−
R_{work}/R_{free} (%)[c]	20.0/26.3	22.7/27.0	23.4/27.5
rmsd for bonds/angles (Å/deg)	0.011/1.45	0.009/1.55	0.010/1.51

[a] Completeness, R_m, and $\langle I/\sigma(I)\rangle$ are given for all data and for data in the highest-resolution shell. [b] $R_m = \Sigma|I - \langle I\rangle|/\Sigma I$, where I is the intensity for individual reflections and $\langle I\rangle$ is the mean intensity of that reflection. [c] $R_{work} = \Sigma||F_o| - |F_c||/\Sigma|F_o|$, where F_o and F_c are the observed and calculated structure factors, respectively. R_{free} was calculated using a test set of 10% of the data.

correct processing of the initiating methionine. N-Terminal sequencing also confirmed that the initiating methionine was removed (data not shown).

Crystallography of the MIF−HPP Complex. To define the structural basis of the enzymatic activity of MIF, soaking and cocrystallization experiments with a variety of substrates and inhibitors were attempted. Soaking experiments with crystals of MIF were unsuccessful. Cocrystallization experiments with MIF under conditions that produced the initial uncomplexed crystals were also unsuccessful. However, we were able to cocrystallize *p*-hydroxyphenylpyruvate with MIF under novel crystallization conditions.

The structure of the orthorhombic crystal form was determined by molecular replacement using the uncomplexed monomer MIF as the search model (*31*). The cross-rotation and translation functions were calculated with AMORE (*30*) using data from 10 to 4 Å resolution. The solution with the highest correlation coefficient had an *R*-factor of 51.6%. Two additional solutions had similar correlation coefficients and *R*-factors and corresponded to the two other subunits in the asymmetric unit. The monomer was refined with X-PLOR using noncrystallographic symmetry constraints against 2.5 Å resolution data. The enol form of hydroxyphenylpyruvate was built into a $2F_o - F_c$ map and subjected to additional refinement. Very large *B*-factors were noted for the substrate when an initial round of *B*-factor refinement was performed. The source of these large *B*-factors was presumed to be either low occupancy of the substrate or the interconversion of the keto and enol forms in the active site. Occupancy refinement was therefore performed on the enol form of HPP which led to an occupancy of 0.43. Subsequent *B*-factor refinement led to *B*-factors of HPP that were comparable to those of the protein. Since both the keto and enol forms are expected to be present during crystallization and data collection, the keto form was also modeled and refined. However, the keto form did not fit into the density as well as the enol form. The final structure has a crystallographic *R*-factor of 20.0% and an R_{free} of 26.3%. The final model was subjected to Luzzati analysis and determined to have coordinate errors of approximately 0.30 Å. A comparison of the uncomplexed

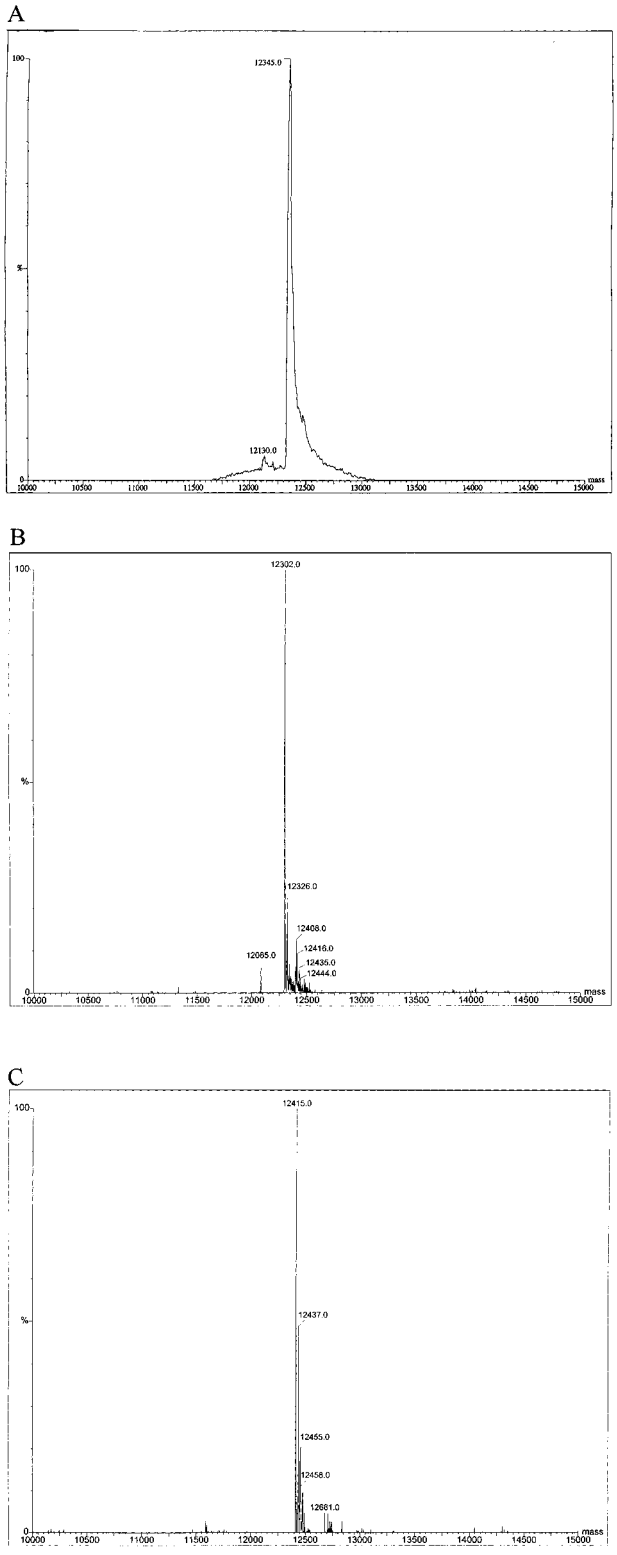

FIGURE 1: Mass spectra of (A) wild-type MIF, (B) P1G, and (C) PAM. The major peak corresponds to the molecular masses for the monomer of MIF: 12 345, 12 302, and 12 415 Da, respectively. These values are all within 2.5 Da of the predicted molecular mass for each protein assuming correct processing of the initiating methionine.

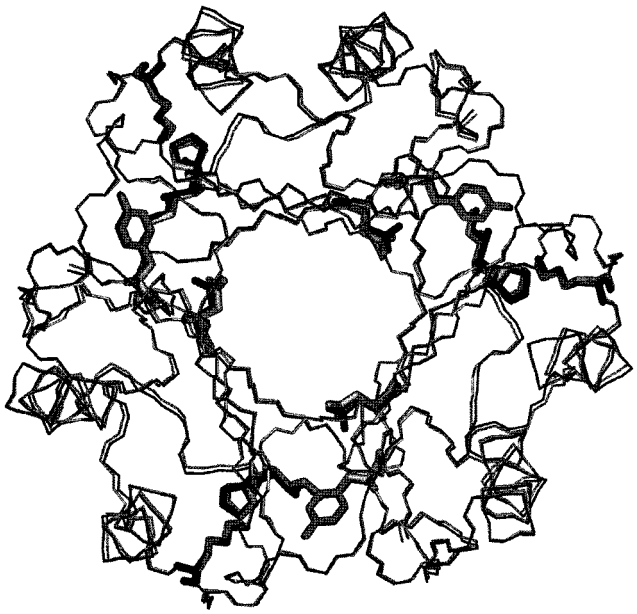

FIGURE 2: Superposition of uncomplexed MIF and MIF−HPP. Backbone atom traces are shown for the trimeric arrangement of uncomplexed MIF (black) and MIF−HPP (gray). All atoms from the active site residues (Pro-1, Lys-32, Ile-64, Tyr-95, and Asn-97) are also displayed. This superposition reveals that there are no major conformational changes upon substrate (not shown) binding. This figure was prepared with the program INSIGHTII (Molecular Simulations, Inc., San Diego, CA).

(*31*) and HPP-complexed MIF structures reveals that there are no major conformational changes that occur upon substrate binding (Figure 2). As in the case of 4-OT and CHMI, binding of the substrate occurs at the interface between the subunits.

Interaction of Hydroxyphenylpyruvate with Active Site Residues. Figure 3A shows a simulated annealing omit map of HPP in the active site with the enol form placed in the electron density. Figure 3B shows the interactions between the enol form of HPP and MIF. The structure of HPP in the active site demonstrates how binding and catalysis occur. A series of aromatic−aromatic interactions, hydrogen bonds, and van der Waals contacts provide the binding energy for HPP. Interestingly, many of these interactions are due to residues from an adjacent subunit, confirming the trimeric nature of the catalytically active state of MIF. The phenyl ring of HPP forms a "Burley" bond with the aromatic ring of Tyr-95C (where C refers to an adjacent subunit) in which the aromatic rings are stacked perpendicular to each other to yield favorable charge−charge interactions that are based on polarization of the aromatic rings (*37*). Interestingly, the hydroxyl group of Tyr-95C is too far from the enol hydroxyl (or keto oxygen) to form a hydrogen bond interaction. There are no other functional groups in proximity to interact with the substrate oxygen. The phenolic hydroxyl group of HPP forms a bifurcated hydrogen bond with the side chain amide nitrogen and carbonyl oxygen of Asn-97C. The binding orientation of HPP in the active site is such that the putative catalytic base, the secondary amine of Pro-1, is within 3.3 Å of C3 from HPP, which would allow for facile proton transfer. The backbone nitrogen of Ile-64 and the side chain nitrogen from Lys-32 are both within hydrogen bonding distance of the carboxylate oxygens of HPP. It is interesting to note that less than 10% of the residues among all MIF

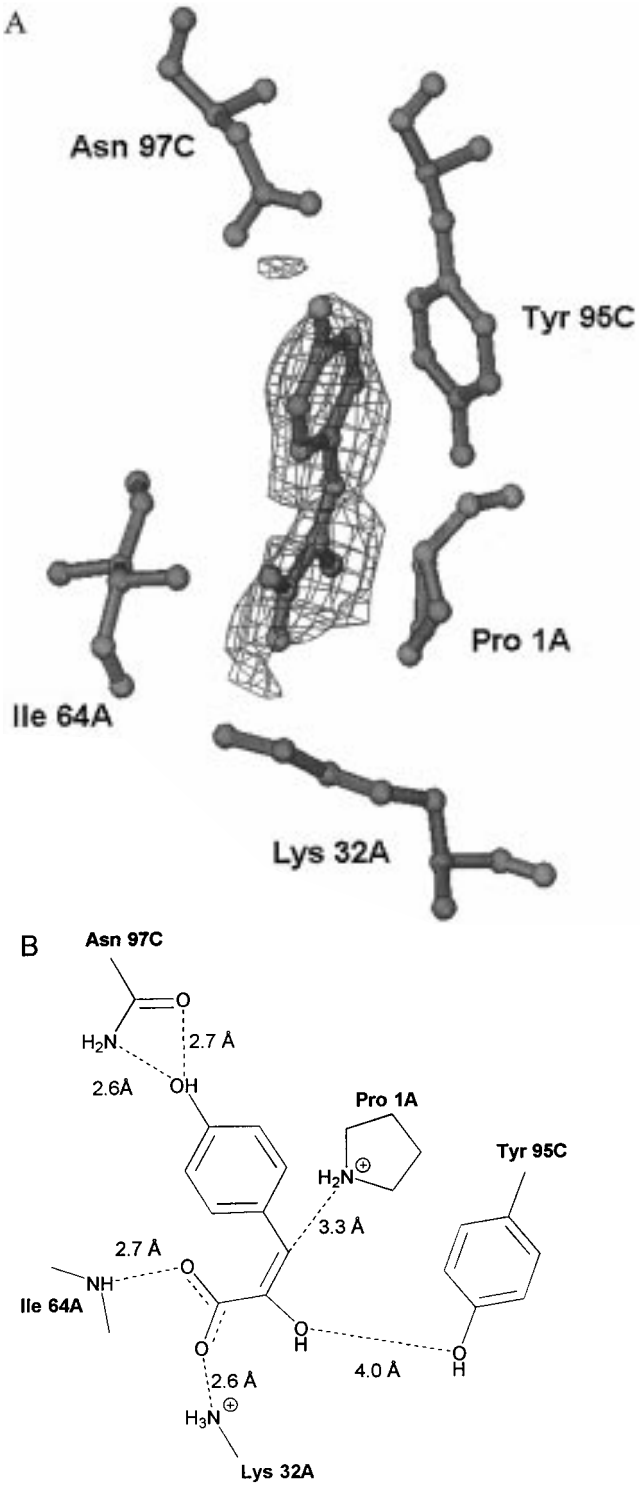

FIGURE 3: Structure and interactions of *p*-hydroxyphenylpyruvate (HPP) and MIF. (A) A $2F_o - F_c$ simulated annealing omit map for HPP in the active site. The enol form of HPP is modeled in the electron density. This figure was created with O (*34*). (B) Schematic of the interactions between protein residues and the enol form of HPP. All distances, with the exception of Tyr-95C, represent hydrogen bonds. Pro-1A, Lys-32A, and Ile-64A are from one subunit, and Tyr-95C and Asn-97C are from an adjacent subunit. Since the enol form is modeled in the active site, Pro-1 is shown to be protonated. The structure demonstrates how binding and catalysis occur. This figure was created with ChemDraw (CambridgeSoft Corp., Cambridge, MA).

homologues are invariant. The key residues involved in the catalytic component of the reaction, Pro-1, Lys-32, and Ile-

64, are among these invariant residues. While Tyr-95 and Asn-97 are not invariant, they are frequently found at their positions or are replaced by conserved residues (*23*).

Catalytic Activity of Pro-1 Mutants. Catalytic assays were performed with P1G and PAM mutants to derive steady state parameters for comparison to those of the wild-type MIF. Both P1G and PAM had undetectable HPP tautomerase activity at the protein concentration (10 nM) that was used to determine the initial rates for the wild-type protein. Therefore, the concentration of each mutant was increased. For the P1G and PAM mutants, the catalytic activity could be measured at approximately 1 and 10 μM, respectively. The levels of HPP tautomerase activity for these two mutants compared to that of the wild-type protein are shown in Figure 4A−C. The kinetic values for wild-type and mutant MIF proteins are listed in Table 2. $[S]_{0.5}$ values are reported because MIF kinetics do not fit the Michaelis−Menten model of kinetics. In contrast to the expected hyperbolic curve typical of Michaelis−Menten kinetics, MIF exhibits a more sigmoidal-shaped curve. Therefore, K_M values cannot be determined. The concentration representing $^1/_2V_{max}$ for the phenylpyruvate tautomerase activity of MIF has been previously reported as K_M, but $[S]_{0.5}$ is a more appropriate designation. P1G has a significantly lower k_{cat}, but a $[S]_{0.5}$ value that is comparable to that of wild-type MIF. PAM has an even lower k_{cat}, but still has a comparable $[S]_{0.5}$. The values of the pseudo-second-order rate constant $k_{cat}/[S]_{0.5}$ of P1G and PAM are 1.5 and <0.1% of the wild-type value, respectively.

pK_a Studies of Pro-1 Mutants. In a previous study, the pK_a of Pro-1 for the wild-type protein was found to be 5.6, almost 4 pH units lower than the pK_a of a proline amide (*23*). The value is similar to the pK_a determined by kinetic analysis and affinity labeling with 3-bromopyruvate (*24*). Here, a similar ^{15}N NMR pH titration study was performed to determine the pK_a of the N-terminus of PAM. As in the wild-type protein, the chemical shift of the N-terminal nitrogen of PAM is well-resolved from all other peaks (Figure 5). The chemical shift of the N-terminal proline in the PAM mutant varied between 50 and 55 ppm for pH values between 4.2 and 9.4. The chemical shift of the nitrogen as a function of pH was fit to the equation

$$\delta(\text{ppm})^{\text{app}} = \frac{\delta_1 + \delta_2(10^{\text{pH}-\text{p}K_a})^n}{[(10^{\text{pH}-\text{p}K_a})^n + 1]}$$

where n is the Hill coefficient and δ_1 and δ_2 are the limiting chemical shifts at low and high pH, respectively. The pK_a of the N-terminus for the PAM mutant is 5.04 ± 0.04. Attempts to determine the pK_a of P1G were unsuccessful. The ^{15}N chemical shift of Gly-1 was undetectable at pH values of >5.5, precluding reliable titration studies.

Structural Studies of Pro-1 Mutants. ^{1}H−^{15}N HSQC experiments were initially used to study the structural integrity of P1G and PAM. The HSQC spectrum of both mutants was similar to that of the wild-type protein, indicating that the global architecture of the protein was retained. Changes in some of the chemical shifts were presumed to be due to local changes at the active site (data not shown). To determine the effects of the mutations in greater detail, the structures of P1G and PAM in the uncomplexed state were determined by X-ray crystallography. (Neither of these mutants could be cocrystallized with HPP in the active site.) Identical crystallization condi-

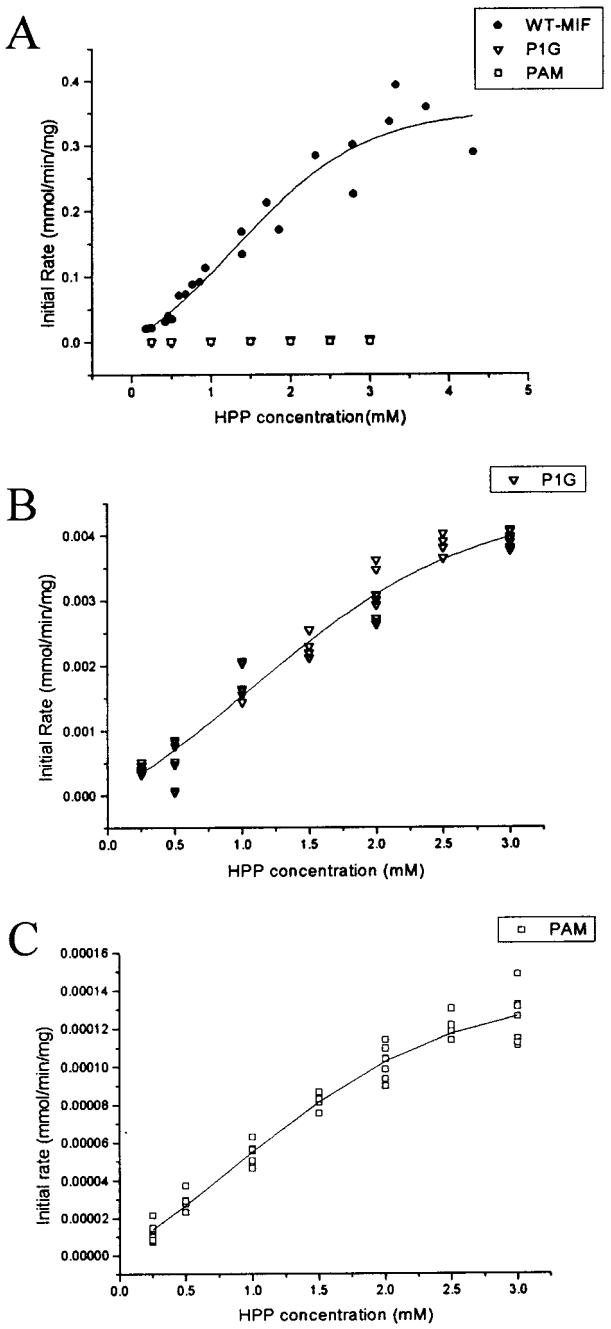

FIGURE 4: Hydroxyphenylpyruvate activity of wild-type and mutant (P1G and PAM) MIF. (A) Relative initial rates (millimoles per minute per milligram plotted against the concentration of HPP) for wild-type MIF (●), P1G (▽), and PAM (□). Initial rates for (B) P1G and (C) PAM. The activity of P1G is significantly reduced compared to that of the wild type, and the activity of PAM is even further reduced. Each curve was fit with a nonlinear Boltzman function to produce a sigmoidal curve using Microcal Origin (Microcal Software, Northampton, MA).

Table 2: Hydroxyphenylpyruvate Tautomerase Activity Kinetic Values

protein	V_{max} (mmol min^{-1} mg^{-1})	k_{cat} (s^{-1})	$[S]_{0.5}$ (mM)	$k_{cat}/[S]_{0.5}$ (M^{-1} s^{-1})
MIF	0.36 ± 0.02	75.83	1.30 ± 0.45	5.83×10^4
P1G	$(4.5 \pm 0.3) \times 10^{-3}$	0.93	1.05 ± 0.27	8.94×10^2
PAM	$(1.4 \pm 0.1) \times 10^{-4}$	0.03	0.84 ± 0.36	3.57×10^1

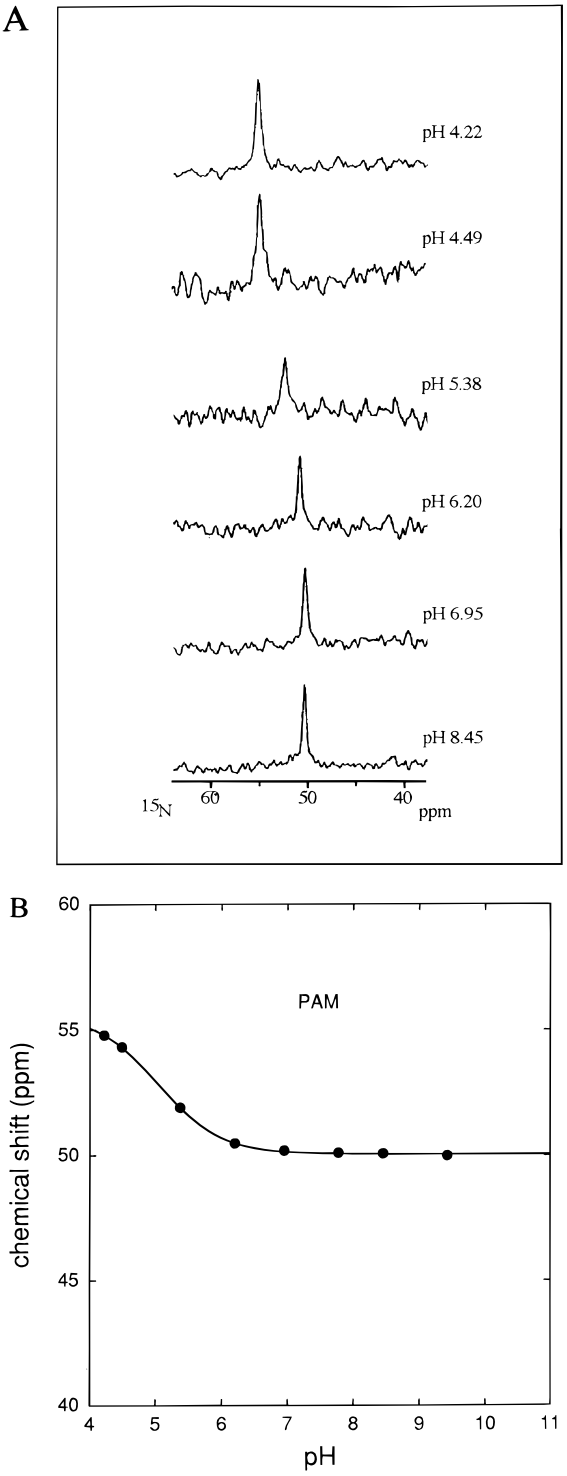

FIGURE 5: pK_a determination of the N-terminal proline in PAM using ^{15}N NMR. (A) Stacked ^{15}N NMR spectrum obtained for MIF at six pH values ranging from 4.22 to 8.45. (B) Titration curve for the pH-dependent ^{15}N chemical shift of the N-terminal proline. The curve was generated from a nonlinear least-squares fit of the data using SigmaPlot (Jandel Scientific) and defines the pK_a of the proline as 5.04 ± 0.04.

tions for the two mutants resulted in different crystal forms; P1G crystallized in the trigonal space group of the wild-type protein, and PAM crystallized in the orthorhombic space group of the wild-type MIF−HPP complex. The mutant structures were determined by difference Fourier methods using phases based on the polypeptides (without the N-terminal residue) in the MIF−HPP complex (for PAM) or uncomplexed MIF (for P1G). The N-terminal residue for each mutant was built and refined to the limit of resolution. The final R_{free} values for the PAM (to 2.0 Å) and P1G (to 2.5 Å) structures are 27.5 and 27.0%, respectively. Estimates of coordinate errors based on Luzzati analysis are 0.25 and 0.32 for PAM and P1G, respectively.

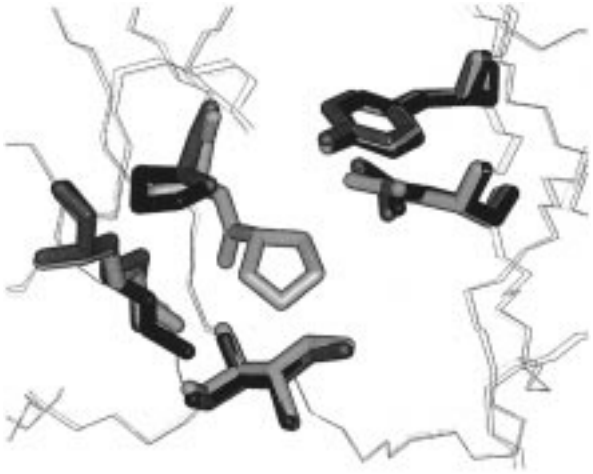

FIGURE 6: Superposition of uncomplexed MIF (black), P1G (dark gray), and PAM (light gray). α-Carbon traces are shown with the residues from one active site displayed. Wild-type MIF and P1G are virtually superimposable, whereas the proline nitrogen of PAM is shifted approximately 3.8 Å from that of the wild type.

As expected, both P1G and PAM have the same overall structure as the wild-type protein (*31*). The only significant change occurs in the active site. Figure 6 shows the superposition of the active site regions of wild-type MIF, P1G, and PAM. The nitrogen of Gly-1 in the P1G mutant is essentially in the same position as that of the nitrogen of the proline in the wild-type structure. The nitrogen of Pro-1 in the PAM structure has shifted by approximately 3.8 Å. These changes are consistent with the relative activity of each mutant. The small change in P1G has a 65-fold effect on $k_{cat}/[S]_{0.5}$, but does not alter the cavity into which HPP binds. In contrast, the insertion of an alanine between Pro-1 and Met-2 pushes proline into the binding site for HPP. On the basis of this structure, it appears unlikely that HPP could bind to PAM in an orientation similar to that of wild-type MIF.

The large movement of the nitrogen in the PAM mutant is also consistent with the decrease in pK_a. The pK_a of a positively charged group is lowered if it is in an area of positive potential and/or in a hydrophobic environment. Analysis of the wild-type structure indicated that Pro-1 is at the base of a hydrophobic cleft (*23*). The environment of this cleft may be subject to the positive potential emanating from Lys-32 and Lys-66. Movement of Pro-1 out of the hydrophobic cleft places the N-terminal proline closer to the source of positive potential and further reduces its pK_a. In wild-type MIF, the distances from the amine of Pro-1 to Lys-32 and Lys-66 are 5.8 and 10.4 Å, respectively. In the PAM mutant, the distances from the N-terminal proline to Lys-32 and Lys-66 are 3.0 and 8.8 Å, respectively. Therefore, the proline in PAM is closer to the positively charged residues, resulting in a reduced pK_a.

DISCUSSION

To resolve the function of Pro-1 in the catalytic activities of MIF, we determined the structure of MIF with a substrate

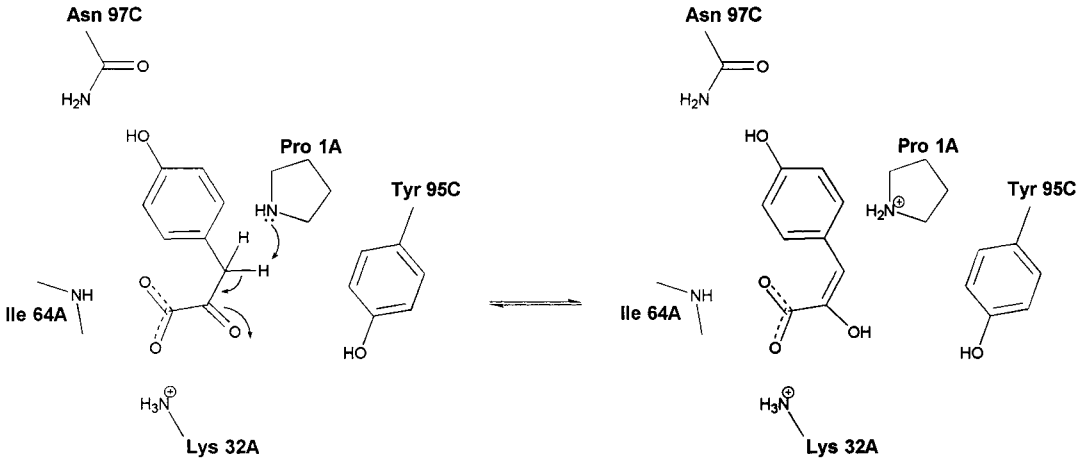

FIGURE 7: Schematic mechanism of MIF-catalyzed keto−enol tautomerase of *p*-hydroxyphenylpyruvate. The secondary amine of Pro-1 is positioned to abstract the *pro-R* proton from C3 of HPP. The active site residues provide hydrogen bonding and other interactions to stabilize HPP within the active site of MIF.

and characterized the kinetic, biochemical, and structural properties of two Pro-1 mutants. The determination of the structure of HPP complexed to MIF confirms the results of our previous studies based on $^{1}H-^{15}N$ HSQC experiments that HPP binds near Pro-1 (*23*). In this study, we characterize the interactions between the substrate and enzyme and propose a reaction mechanism (Figure 7). Several hydrogen bonding interactions between HPP and MIF help to orient HPP within the active site. The secondary amine of Pro-1 is positioned to abstract the proton from C3. In many reactions involving abstraction of a proton adjacent to an α-keto acid, the C−H bond is weakened by a general acid or functional group that polarizes the adjacent carbonyl oxygen (*38*). In MIF, there is no such functional group for hydroxyphenylpyruvate. In contrast, Arg-39 of 4-OT is believed to polarize the carbonyl oxygen by functioning as a general acid in the isomerization of 2-oxo-4-hexenedioate to 2-oxo-3-hexenedioate (*39*). Although Tyr-95 of MIF occupies a position similar to that of Arg-39 in 4-OT, the hydroxyl group of Tyr-95 is too far away from the carbonyl oxygen of HPP to form a hydrogen bond. This suggests that Tyr-95 may play a role similar to that of Arg-39 in 4-OT in the uncharacterized physiological catalytic reaction of MIF and helps to explain the low catalytic rate of the MIF phenylpyruvate tautomerase reaction relative to the near diffusion-controlled rate of 4-OT.

Previously published mechanistic studies of the phenylpyruvate tautomerase reaction (*40*, *41*) were reported long before MIF was discovered to be responsible for this activity (*16*). The *pro-R* methylene hydrogen was specifically removed and exchanged with solvent protons (*40*). From a study involving differential inhibition data of stereoisomeric vinyl fluoride inhibitors, the configuration of the enol was assigned to be (*E*) rather than the more thermodynamically favorable (in solution) (*Z*) isomer (*41*). Our studies add further support to the belief that the phenylpyruvate tautomerase that had been studied is MIF and put the published results in a structural context. HPP in the active site of MIF adopts the (*E*) configuration due to the interactions shown in Figure 3B. Pro-1 is poised to abstract the *pro-R* methylene proton.

The three-dimensional structure of the MIF−HPP complex is also significant because it provides further support for the trimeric nature of the catalytically active protein. The oligomerization state of MIF had been a source of controversy prior to the determination of the three-dimensional structure. The trimeric nature found in the crystal did not totally resolve the controversy due to the possibility that it was an artifact of crystallization or high protein concentration. Results from various NMR (*23*, *42*), biochemical (*25*), and mutagenesis (*43*) experiments have also supported the significance of the trimeric form. The presence of interactions with HPP from two different subunits now confirms the trimeric arrangement of MIF for its catalytic function.

Investigation of the catalytic activities and structures of two MIF mutants yields further insight into the precise mechanism of phenylpyruvate tautomerase activity. Mass spectroscopy and N-terminal sequencing confirmed that both the PAM and P1G mutants do not contain an N-terminal methionine, which might have interfered with the interpretation of the results. X-ray crystallography shows that the PAM and P1G mutants exhibit no major structural changes as compared to the wild-type enzyme. Therefore, all changes in catalytic activity are due to changes in the active sites of the mutants. The PAM mutant, in which an alanine is inserted between Pro-1 and Met-2, exhibits minimal catalytic capacity. This is similar to a mutant for 4-oxalocrotonate tautomerase, which was severely impaired but had residual activity when its N-terminus was inadvertently extended by one amino acid (*44*). The movement of Pro-1 toward the solvent decreases its pK_a from 5.6 to 5.0. This reduction in pK_a for the catalytic base may partly explain the decrease in activity based on the Brønsted relationship, but the three-dimensional structure suggests a more likely explanation. The proline of PAM occupies a position that would normally be occupied by the substrate. It is therefore more plausible that the residual catalytic activity for this mutant is due to an entirely different mechanism.

The P1G mutant has significant catalytic activity. There is only a small decrease in $[S]_{0.5}$, but an 82-fold reduction in k_{cat}. One possible source of the reduced activity is a decrease in pK_a for the catalytic base. It was not possible to measure the pK_a due to the inability to monitor the chemical shift of Gly-1 across the pH spectrum. However, assuming the change in pK_a at the active site is similar to the relative difference in pK_a between proline and glycine (0.8 unit) (*45*),

we can estimate a pK_a of 4.8 for P1G. Such an estimate is justified since there are no major structural changes in the active site of P1G (relative to wild-type MIF) that would lead to an unusual difference in pK_a for these two residues. This difference is also consistent with the observed pK_a difference between the P1G mutant and wild-type 4-oxalocrotonate tautomerase (*44*). The pK_a difference is therefore only due to the inherent difference in pK_a between a primary and secondary amine. On the basis of the Brønsted relationship, the lower basicity of the catalytic base due to the estimated change in pK_a does not fully account for the decrease in k_{cat}. The conformational flexibility of glycine compared to the rigidity of proline is likely to account for the remaining decrease. Proton abstraction is very sensitive to the distances and geometry between base and acid (*46*). The increased flexibility of glycine during the transition state of the reaction may play a key role in reducing the catalytic activity of P1G.

It appears likely that nature has chosen a proline as the catalytic base for MIF, 4-OT, and CHMI for the rigidity it imposes on the amine group rather than for its unique pK_a relative to the other amino acids. It is clear from the dramatic difference in the pK_a of proline in these enzymes relative to that of proline amide that nature could fine-tune whatever pK_a is required. However, imposing rigidity on the catalytic base during the transition state in the context of an active site that requires some flexibility to allow substrate binding must be a more difficult task. The only amino acid that allows nature to achieve its requirement for rigidity is proline.

ACKNOWLEDGMENT

We thank Paul Pepin for technical assistance, Walter McMurray for mass spectrometric analysis, the Keck Foundation Biotechnology Resource Laboratory at Yale University for DNA and N-terminal sequencing, Chris Whitman for useful discussions, and Karen Anderson for critical reading of the manuscript.

REFERENCES

1. Bernhagen, J., Calandra, T., and Bucala, R. (1998) *J. Mol. Med. 76*, 151−161.
2. Bucala, R. (1996) *Cytokine Growth Factor Rev. 7*, 19−24.
3. Calandra, T., and Bucala, R. (1997) *Crit. Rev. Immunol. 17*, 77−88.
4. Metz, C., and Bucala, R. (1997) *Adv. Immunol. 66*, 197−223.
5. Bloom, B. R., and Bennett, B. (1966) *Science 153*, 80−82.
6. David, J. (1966) *Proc. Natl. Acad. Sci. U.S.A. 56*, 72−77.
7. Bernhagen, J., Bacher, M., Calandra, T., Metz, C. N., Doty, S. B., Donnelly, T., and Bucala, R. (1996) *J. Exp. Med. 183*, 277−282.
8. Calandra, T., and Bucala, R. (1995) *J. Inflammation 47*, 39−51.
9. Bernhagen, J., Calandra, T., Mitchell, R. A., Martin, S. B., Tracey, K. J., Voelter, W., Manogue, K. R., Cerami, A., and Bucala, R. (1993) *Nature 365*, 756−759.
10. Calandra, T., Speigel, L. A., Metz, C. H., and Bucala, R. H. (1998) *Proc. Natl. Acad. Sci. U.S.A. 95*, 11383−11388.
11. Donnelly, S. C., and Bucala, R. (1997) *Mol. Med. Today 3*, 502−507.
12. Mikulowska, A., Metz, C. N., Bucala, R., and Holmdahl, R. (1997) *J. Immunol. 158*, 5514−5517.
13. Lan, H. Y., Bacher, M., Yang, N., Mu, W., Nikolic-Paterson, D. J., Metz, C., Meinhardt, A., Bucala, R., and Atkins, R. C. (1997) *J. Exp. Med. 185*, 1455−1465.
14. Bozza, M., Satoskar, A. R., Lin, G., Lu, B., Humbles, A. A., Gerard, C., and David, J. R. (1999) *J. Exp. Med. 189*, 341−346.
15. Rosengren, E., Bucala, R., Aman, P., Jacobsson, L., Odh, G., Metz, C. N., and Rorsman, H. (1996) *Mol. Med. 2*, 143−149.
16. Rosengren, E., Aman, P., Thelin, S., Hansson, C., Ahlfors, S., Bjork, P., Jacobsson, L., and Rorsman, H. (1997) *FEBS Lett. 417*, 85−88.
17. Kleemann, R., Kapurniotu, A., Frank, R. W., Gessner, A., Mischke, R., Flieger, O., Juttner, S., Brunner, H., and Bernhagen, J. (1998) *J. Mol. Biol. 280*, 85−102.
18. Lolis, E., and Bucala, R. (1996) *Proc. Assoc. Am. Physicians 108*, 415−419.
19. Suzuki, M., Sugimoto, H., Nakagawa, A., Tenaka, I., Nishihira, J., and Sakai, M. (1996) *Nat. Struct. Biol. 3*, 259−266.
20. Subramanya, H. S., Roper, D. I., Dauter, Z., Dodson, E. J., Davies, G. J., Wilson, K. S., and Wigley, D. B. (1996) *Biochemistry 35*, 792−802.
21. Stivers, J. T., Abeygunawardana, C., Mildvan, A. S., Hajipour, G., Whitman, C. P., and Chen, L. H. (1996) *Biochemistry 35*, 803−813.
22. Stivers, J. T., Abeygunawardana, C., Mildvan, A. S., Hajipour, G., and Whitman, C. P. (1996) *Biochemistry 35*, 814−823.
23. Swope, M., Sun, H. W., Blake, P. R., and Lolis, E. (1998) *EMBO J. 17*, 3534−3541.
24. Stamps, S. L., Fitzgerald, M. C., and Whitman, C. P. (1998) *Biochemistry 37*, 10195−10202.
25. Bendrat, K., Al-Abed, Y., Callaway, D. J., Peng, T., Calandra, T., Metz, C. N., and Bucala, R. (1997) *Biochemistry 36*, 15356−15362.
26. Sambrook, J., Fritsch, E. F., and Maniatis, T. (1989) *Molecular Cloning: A Laboratory Manual*, 2nd ed., Cold Spring Harbor Laboratory Press, Cold Spring Harbor, NY.
27. Sun, H. W., Swope, M., Cinquina, C., Bedarkar, S., Bernhagen, J., Bucala, R., and Lolis, E. (1996) *Protein Eng. 9*, 631−635.
28. Otwinowski, Z., and Minor, W. (1997) *Methods Enzymol. 276*, 307−325.
29. Dodson, E. J., Winn, M., and Ralph, A. (1997) *Methods Enzymol. 277*, 620−633.
30. Navaza, J. (1994) *Acta Crystallogr. A50*, 157−163.
31. Sun, H. W., Bernhagen, J., Bucala, R., and Lolis, E. (1996) *Proc. Natl. Acad. Sci. U.S.A. 93*, 5191−5196.
32. Brünger, A. T. (1997) *X-PLOR*, Yale University Press, New Haven, CT.
33. Brünger, A. T. (1992) *Nature 355*, 472−475.
34. Jones, T. A., Zou, J. Y., Cowan, S. W., and Kjeldgaard, M. (1991) *Acta Crystallogr. A47*, 110−119.
35. Kleywegt, G. J., and Jones, T. A. (1995) *Structure 3*, 535−540.
36. Luzzati, V. (1952) *Acta Crystallogr. 5*, 808−810.
37. Burley, S. K., and Petsko, G. A. (1985) *Science 229*, 23−28.
38. Gerlt, J. A., and Gassman, P. G. (1992) *J. Am. Chem. Soc. 114*, 5928−5934.
39. Taylor, A. B., Czerwinski, R. M., Johnson, W. H., Whitman, C. P., and Hackert, M. L. (1998) *Biochemistry 37*, 14692−14700.
40. Retey, J. (1977) *Eur. J. Biochem. 72*, 251−257.
41. Pirrung, M. C., Chen, J., Rowley, E. G., and McPhail, A. T. (1993) *J. Am. Chem. Soc. 115*, 7103−7110.
42. Muhlhahn, P., Bernhagen, J., Czisch, M., Georgescu, J., Renner, C., Ross, A., Bucala, R., and Holak, T. A. (1996) *Protein Sci. 5*, 2095−2103.
43. Kleemann, R., Mischke, R., Kapurniotu, A., Brunner, H., and Bernhagen, J. (1998) *FEBS Lett. 430*, 191−196.
44. Czerwinski, R. M., Johnson, W. H., Jr., and Whitman, C. P. (1997) *Biochemistry 36*, 14551−14560.
45. Dawson, R. M. C., Elliott, D. C., Elliott, W. H., and Jones, K. M. (1986) *Data for Biochemical Research*, 3rd ed., Clarendon Press, Oxford, U.K.
46. Joseph-McCarthy, D., Rost, L. E., Komives, E. A., and Petsko, G. A. (1994) *Biochemistry 33*, 2824−2829.

BI990306M